Chapter 11

Fracture Analysis of Generator Fan Blades

Mahmood Sameezadeh and Hassan Farhangi

Additional information is available at the end of the chapter

http://dx.doi.org/10.5772/54122

1. Introduction

Critical gas turbine rotating component, such as turbine blades, compressor disks, spacers and cooling fan blades are subjected to cyclic stresses during engine start-up, operation and shut-down. The lifetime of these components are usually established on the basis of probabilistic crack initiation criterion for a known fracture-critical location (Koul & Dainty, 1992). Therefore, periodic inspections are carried out to detect the probable cracks and prevent suddenly fractures.

Shaft driven rotating fans are commonly utilized to provide the required cooling for generators. These fans circulate cooling gas, air or hydrogen, throughout the machine to maintain the electrical windings at safe operating temperatures. Cooling air is circulated in a closed cycle, in a way that after passage of air through rotor, it is heated and exhausted from top of the generator, which then passes through a cooler, which would cool it down using water flow. Cool air again flows towards rotor and by use of fans, which are installed on retaining ring at the generator sides, is blown around the rotor. Each fan is comprised of several blades, which have been separated by using spacers. In Fig. 1, overall plan of generator and air cycle is shown (Moussavi et al., 2009).

Failure of a rotating fan inside a generator will cause extensive damage. The stored rotational energy in a fan that lets loose will typically destroy the stator winding, sometimes damage the stator core and cause damage to other rotor components such as retaining rings, the rotor winding and possibly even the rotor forging (Moore, 2002). Fan blades are regularly inspected during overhauls by visual and dye penetrant inspections and are required to be replaced due to defects caused by crack, corrosion and impact.

This chapter reports the failure investigation of a rotating axial flow fan of the Iran Montazer-Ghaem-VI 123 MW capacity generator unit. The unit was equipped with two rotating fans, one at each end namely at the turbine side and the exciter side of the generator. The failed fan consisting of 11 blades was mounted on the generator-rotor at the

turbine end, and had a total service life of about 41000 hours prior to the failure. The fan rotational speed was 3000 revolutions per minute (rpm) and the maximum operating temperature of the blades was 90°C.

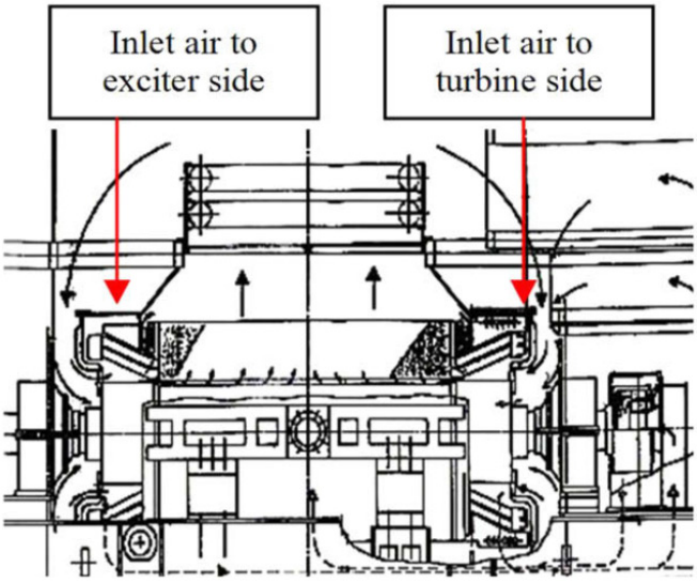

Figure 1. Generator diagram (Moussavi et al., 2009)

Initial investigation pointed out that three blades were fractured and several others were cracked just about 11 hours after resuming operation following the last major overhaul, causing extensive damage to the generator unit specially the stator windings. The failure of the blades was investigated using fractographic and microstructural characterization techniques as well as mechanical evaluations to identify the root cause of the failure. Two similar failures at this kind of fan that caused extensive damage to generator units have been reported from Iran. After some investigations, the corresponding company changed the mounting angle of blades from 19º to 14º to solve the problem of the fans (Iran Power Plant Repair Comany [IPPRC], 2003, 2004).

2. Experimental procedure

Visual inspections were taken on the generator parts especially on the fan blades and the effect of accident on them was studied. Three kinds of blades were found in the turbine casing after the accident: fractured blades, cracked blades and un-cracked blades. The failure was at the turbine side of the generator and according to the visual inspections, the fan blades at the excitor side were not damaged. Dye penetrant non-destructive test was used for detection of surface cracks on the blades. Chemical analysis of the fan blade material was conducted using optical emission spectroscopy. Brinell hardness measurements were taken on the sections prepared from the airfoils as well as on the base of all blades. All

measurements were carried out using a 5 mm ball at a load of 1.23 kN. Longitudinal round tensile specimens were machined from the roots and tested according to ASTM E8M. Fatigue specimens were prepared from root of the fractured blades and rotary bending test was done in accordance with DIN 50113.

Longitudinal and transverse specimens were cut from the airfoils for scanning electron microscopy (SEM) and metallography. The metallography samples were prepared by using standard metallographic techniques and etched with modified Keller's reagent. The microstructure of the blade material was analyzed using an optical microscope and an Oxford MV2300 SEM equipped with an energy dispersive spectroscopy (EDS) facility. Fractographic studies were performed using visual examination. Following visual examination of the failed blades, portions of the fracture surfaces were cut for fractographic studies using SEM. All the specimens used for material characterization tests were prepared from the airfoils and bases of the fractured fan blades.

The stresses acting on the blades in steady state condition and at the time of final fracture were estimated using linear elastic fracture mechanics, finite element method (FEM) and fractographic results. At the end, a three-dimensional crack growth software was utilized to assess the crack growth rate and fatigue life in a simplified model of airfoils.

3. Results and discussion

3.1. Visual inspections

Visual inspections indicated that the accident has led to three different categories for the fan blades of the turbine side (Table 1). Dye penetrant testing revealed the cracked blades which did not completely fracture during the accident. A photograph of the fractured blades, labelled in according with their location on the fan is shown in Fig. 2.

All the examinations of mounting clearances, tightening and locking of the blades and the air guide mounting showed no defect also, there were no sign of foreign bodies in the turbine casing.

Category	Blade Number	Specification
Fractured	1, 8, 11	Blade completely fractured and airfoil separated from root
Cracked	2, 3, 7, 9	Including central or edge cracks
Un-cracked	4, 5, 6, 10	Without any surface crack

Table 1. Visual examination of turbine side blades

3.2. Materials characterization

3.2.1. Chemical composition

The chemical composition of the fan blades is given in Table 2. The closest standard aluminum alloy found in the literature is AA 2124 which is a wrought and heat treatable alloy (American Society for Metals [ASM], 1990). This alloy derives its strength mainly from

second phase particles which are distributed in the matrix through a precipitation hardening process.

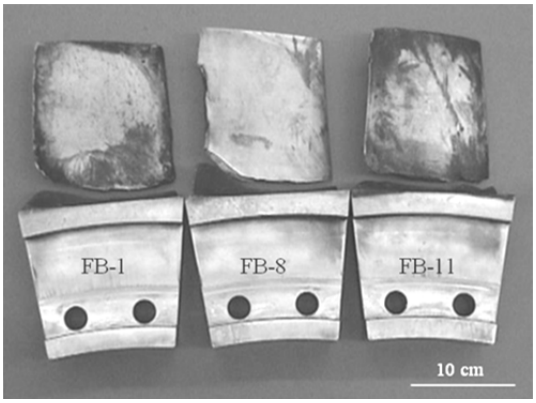

Figure 2. Fractured fan blades

Element / Alloy	Al	Cu	Mg	Mn	Si	Fe	Zn
2124	--Base--	3.8 – 4.9	1.2 – 1.8	0.30 – 0.9	0.20 max	0.30 max	0.25 max
Blade	Base	4.19	1.72	0.62	0.167	0.11	0.03

Table 2. Chemical composition of the fan blade material

3.2.2. Hardness

Brinell macrohardness measurements carried out on different sections of airfoils showed that the hardness was about 133 ± 5 HB, which was essentially uniform along various sections.

3.2.3. Tensile properties

The average values of yield stress, tensile strength, and elongation are 380 MPa, 510 MPa, and 22%, respectively.

The tensile properties and the hardness number of the blades material are all within the standard range reported for Aluminum alloy 2124 (ASM, 1990). The results indicate no degradation in the mechanical properties of the fan blades during service operation.

3.2.4. Fatigue test

The measured lifetime versus applied stress from the rotaty bending fatigue test is presented in Fig. 3. A SEM micrograph taken from the fracture surface of a tested specimen

is shown in Fig. 4. Presence of several second phase particles on the surface is obvious. This kind of large particles can accelerate the fatigue crack initiation and affect the fatigue behaviour of the blade material.

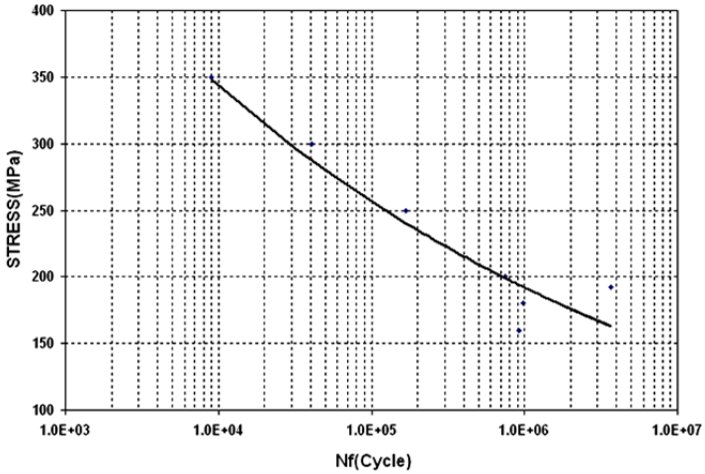

Figure 3. Fatigue test S-N curve

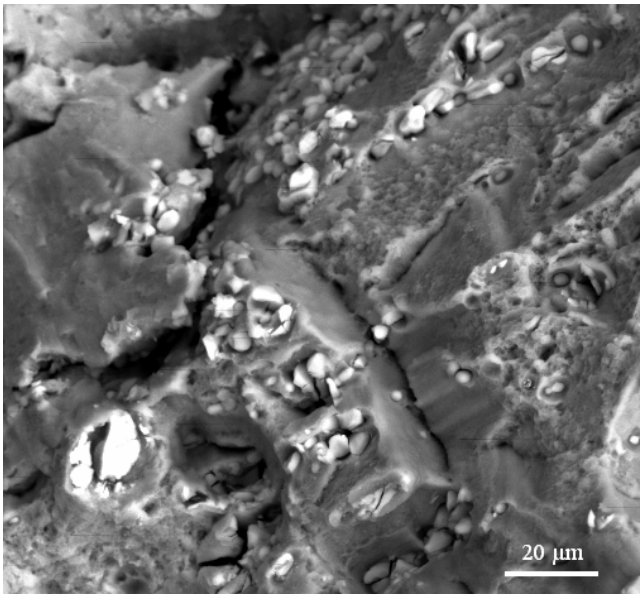

Figure 4. Fracture surface of a fatigue test specimen

3.2.5. Microstructure

Typical microstructures of the blade material in the longitudinal and transverse sections of a cracked airfoil are shown in Fig. 5. The microstructure consists of elongated grains and second phase particles in the longitudinal direction. Various types of second phase particles can be identified in the SEM micrograph, shown in Fig. 6. The large and elongated particle on the micrograph was subjected to EDS analysis. The composition of the particle contained iron, copper and aluminum which is consistent with the β-phase (Al_7Cu_2Fe) particles common to aluminum alloys (Merati, 2005).

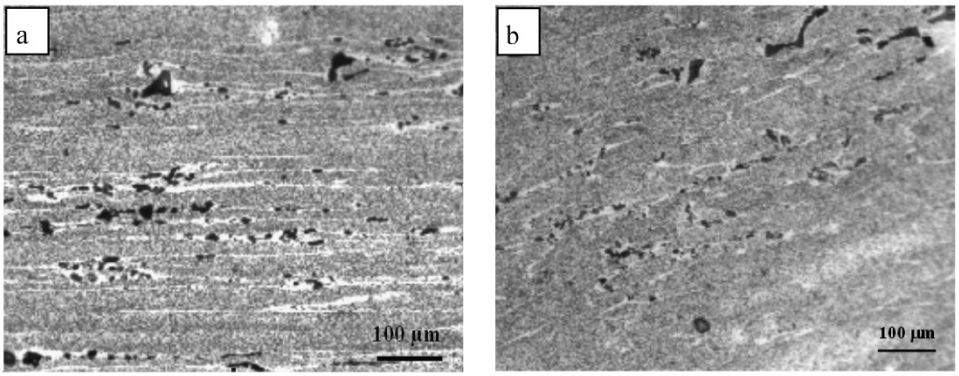

Figure 5. Microstructures of longitudinal (a) and transverse (b) sections of a cracked blade

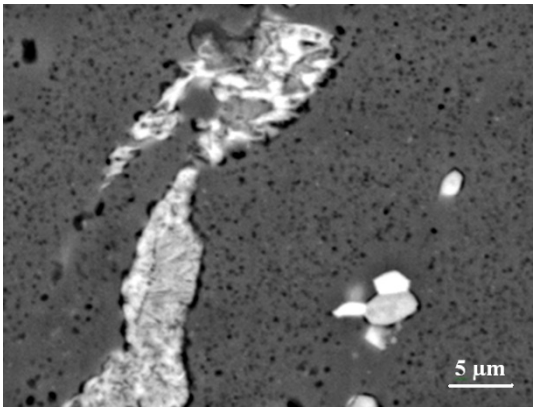

Figure 6. SEM micrograph showing large second phase particles

3.3. Fractography

The fracture location of the broken blades can be identified from Fig. 2. It can be seen that the fracture had occurred close to the transition radius between the blade airfoil and the blade root. All the fracture surfaces exhibited very similar macroscopic features. A

representative fractograph of the fracture surface of blade No. 8 is shown in Fig. 7a. It is observed to consist of two distinct regions at low magnification, a semi-elliptical and smooth region which is oriented normal to the blade axis and exhibits a macroscopically brittle appearance, and an outer region with a rougher and more ductile appearance. The transition from semi-elliptical region to the outer region can be clearly identified in Fig. 7b. In this region the remaining cross section of the blade failed by tensile overload.

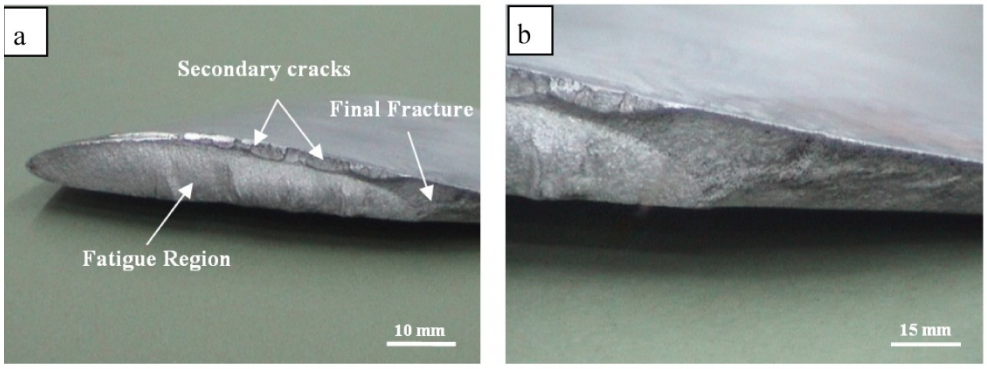

Figure 7. (a) Fracture surface of blade No. 8, (b) transition from fatigue to tensile overload fracture

Faint beach marks indicative of the progressive nature of crack growth in the semi-elliptical region can be seen in Fig. 8. Parallel microscopic fracture surface markings can also be observed in this region at higher magnifications in SEM micrograph as shown in Fig. 9. A schematic drawing of the fan with the location of damaged blades is presented in Fig. 10. Visual inspections and fractographic assessments revealed that the sequence of fracture for the broken blades has been blade No. 1, blade No. 8 and blade No. 11 respectively (Sameezadeh, 2005).

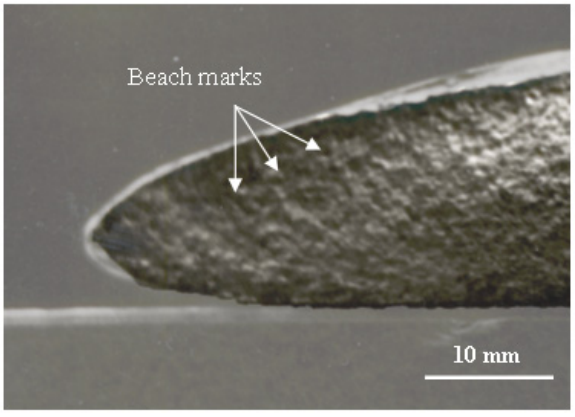

Figure 8. Beach marks on the fracture surface near the leading edge of the blade

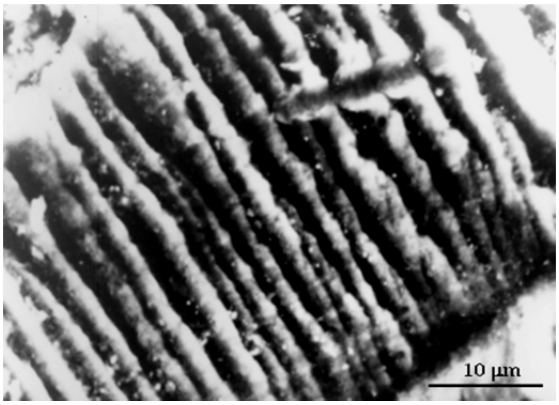

Figure 9. SEM fractograph showing parallel fracture surface markings

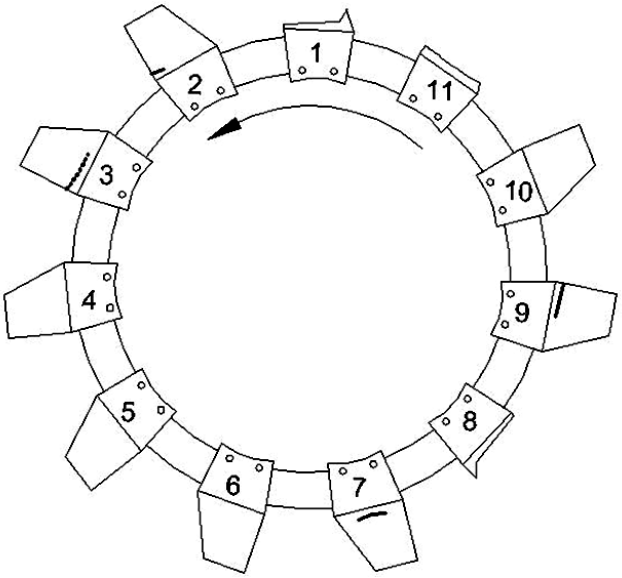

Figure 10. Schematic drawing of the fan with location of damaged blades

Table 3 shows the crack lengths which are measured on the surface of cracked blades. Schematic drawings of the fracture surfaces of three broken fan blades which show multiple crack initiation sites as well as the macroscopic crack growth paths are presented in Fig. 11. Also, For the first and the second fractured blades (blades No. 1 & No. 8), primary crack initiation sites are located on the concave side of the airfoils near the centre where the cross-sectional area is high. Primary cracks have coalesced during fatigue crack growth to form shallow semi-elliptical crack geometry and have propagated to reach the final cracks. In

addition, several small semi-elliptical cracks are also shown to have initiated from the opposite convex side of the airfoils.

Blade No. / Crack location	2	3	7	9
Outer surface	24	3	70	78
Inner surface	79	90	-	80

Table 3. Measured lengths of surface cracks

Based on the fractographic observations, fatigue cracking is singled out as the primary fracture mechanism involved in the failure of the fan blades. Final fracture regions constitute only about 25–30 % of the fracture surfaces of the blades. Therefore, fatigue cracking of the blades can be considered to have occurred under high cycle fatigue conditions.

According to Fig. 11 the presence of shallow semi-elliptical cracks on both concave and convex sides of the airfoils is indicative of the influences of considerable bending stresses during crack propagation.

An SEM micrograph showing one of the typical primary crack initiation sites is presented in Fig. 12a. A secondary electron mode micrograph of this region revealed a large second phase particle with a length of about 100 μm at the crack origin as shown in Fig. 12b. The EDS spectrum of this particle identified that its composition is very similar to the intermetallic particle. Presence of the large particles at the origin of the crack have been shown to act as preferred fatigue crack nucleation sites in such alloys, despite the fact that they represent a small fraction of the particle population (Kung, 1979; Merati, 2005).

Crack propagation mode near the initiation region and throughout the fatigue fracture surface was predominantly transgranular and formation of secondary cracks was very limited. Examination of the airfoils near the crack initiation sites showed no apparent defects due to corrosion or foreign object impact.

Dye penetrant non-destructive testing that was carried out on the blades after the accident identified that some of the non-fractured blades have been cracked. The crack surface of one of these blades (blade No. 7) was disclosed as shown in Fig. 13 by cutting the remaining cross-section of the airfoil and opening carefully. In this figure the semi-elliptical fatigue region is obvious. The crack surface is covered by the penetrant material and a higher magnification view identifies the transition of the penetrant material out of the fatigue region that has different microscopic features, so it can be recognized as the final fracture zone. Therefore, the final fracture stage could not be completed because of the generator stoppage after the fracture of the three blades.

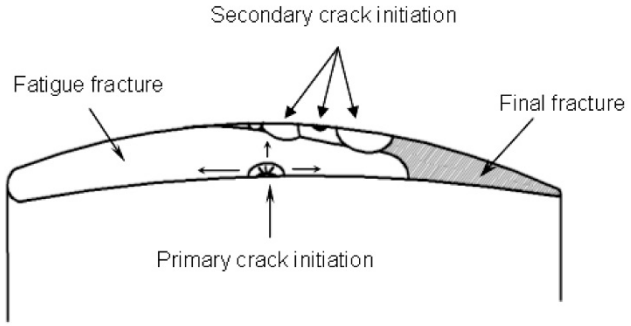

(a)

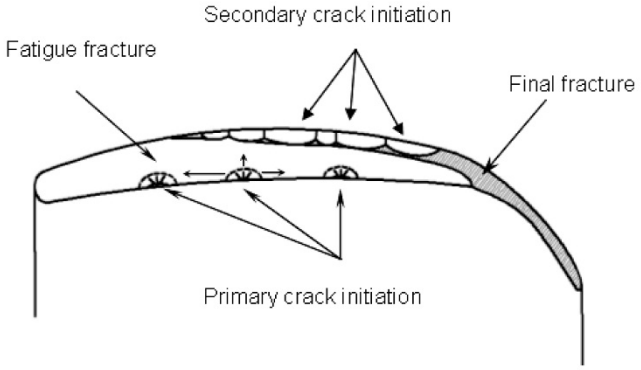

(b)

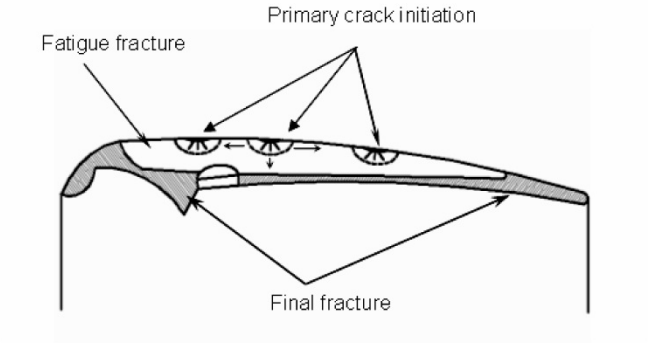

(c)

Figure 11. Schematic drawings of the fracture surfaces: (a) blade No. 1, (b) blade No. 8 and (c) blade No. 11

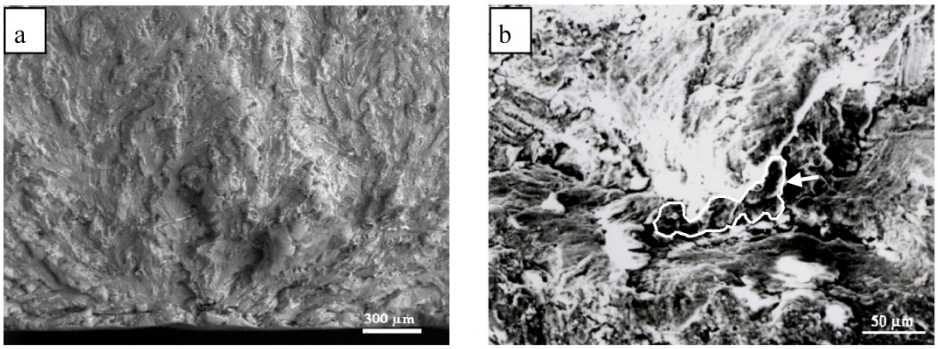

Figure 12. (a) Typical micrograph showing a primary crack initiation site and (b) a crack nucleating particle at the origin of the crack

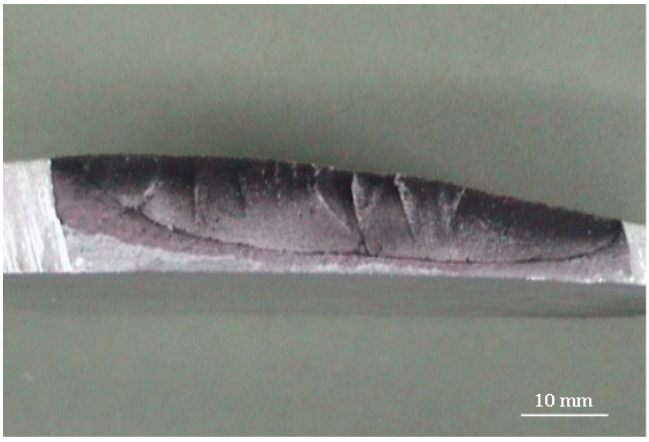

Figure 13. Opened crack surface of blade No. 7

Crack initiation and growth from the convex side and also decrease in the fatigue region in comparison with the fractured blades, prove that the fluctuation of the stresses and the maximum stress had been highly increased during the accident probably due to excessive vibrations.

3.4. Stress analysis of the blades

3.4.1. Steady state stresses

The most important stresses acting at the transition radius in the critical cross-section of the airfoils, under normal operating conditions, consist of a tensile stress component due to centrifugal forces and a bending stress component introduced by the action of the air flow pressure. The tensile stress depends on the rotational speed (N, 50 revolutions per second), mass of the airfoils (m, 0.51 kg), distance from the center of rotation (r, 0.615 m)

and the cross-sectional area (A, 0.00155 m^2) as given by the following expression (Bleier, 1997):

$$\sigma_t = \frac{mr(2\pi N)^2}{A} \tag{1}$$

The tensile stress component due to the centrifugal forces is calculated from the above relationship to be about 20 MPa, which is essentially constant during operation.

A 3D finite element model was used to simulate the normal operation of the fan blades. The results revealed that the maximum total stress acting on the blade under normal condition was about 27 MPa which occurred close to the transition radius between the airfoil and the root where the cracks initiated in fractured blades (Fig. 14) (Ataei, 2006). The bending stress introduced by the action of the air flow pressure are less important (Cohen, 1987) and was estimated as about 7 MPa. According to the results, the steady state stresses are very low in comparison with the strength of the blade material therefore, it can be concluded that the fracture accident was happened during an abnormal condition.

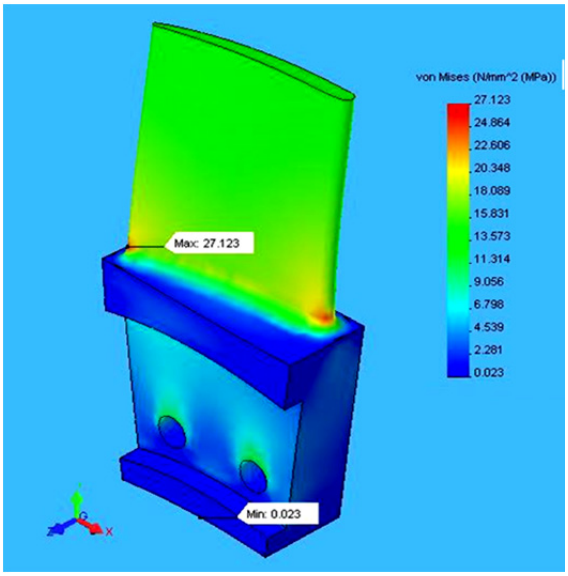

Figure 14. Finite element simulation of the fan blade, which shows the stress distribution under normal operating condition (Ataei, 2006)

3.4.2. Failure stresses

The low aspect ratio of primary fatigue cracks suggests that crack propagation was influenced by significantly higher bending stress levels than that caused by air flow pressure alone. Moreover, since mode I loading condition was dominant and the fatigue crack

growth plane was normal to the tensile stress axis, individual components of stress intensity factors due to tension and bending can be added to obtain the total crack tip stress intensity. Accordingly, the failure stress at the time of final fracture and the magnitude of additional bending stresses which influenced the fatigue cracking process can be estimated by applying the superposition principle and fracture toughness data using the following equation (Anderson, 1995; Broek, 1995):

$$K_{\mathrm{IC}} = K_{\mathrm{t}} + K_{\mathrm{b}} \tag{2}$$

$$K_{\mathrm{IC}} = F\sigma_{\mathrm{t}}\sqrt{\frac{\pi a}{Q}} + FH\sigma_{\mathrm{b}}\sqrt{\frac{\pi a}{Q}} \tag{3}$$

where the fracture toughness of the material was taken as $31.9\ \mathrm{MPa}\sqrt{\mathrm{m}}$ from the literature (ASM, 1990) and the values for F, H and Q geometrical parameters can be calculated for each specific crack geometry under combined tension and bending stresses using Newman–Raju equations (Newman & Raju, 1984).

According to the fractographic results the final fatigue crack of the first broken blade (blade No.1) at the time of final fracture was assumed as a quarter-elliptical corner crack with $a = 12\times10^{-6}$ m and $c = 83\times10^{-6}$ m dimensions, thus the values for F, H and Q parameters in Eq. (3) were calculated as 5.02, 0.20 and 1.07 respectively. Using the above data and a 20 MPa tensile stress, the bending stress can be estimated by the following calculations:

$$K_{\mathrm{t}} = F\sigma_{\mathrm{t}}\sqrt{\frac{\pi a}{Q}} = 18.8\ \ \mathrm{MPa}\sqrt{\mathrm{m}} \tag{4}$$

$$K_{\mathrm{b}} = HF\sigma_{\mathrm{b}}\sqrt{\frac{\pi a}{Q}} = K_{\mathrm{IC}} - K_{\mathrm{t}} = 13.1\ \ \mathrm{MPa}\sqrt{\mathrm{m}} \tag{5}$$

$$\sigma_{\mathrm{b}} = 69.5\ \mathrm{MPa} \tag{6}$$

The bending stress at the time of fracture of the first broken blade was estimated as about 70 MPa and the total stress acting on the airfoil is thus about 90 MPa (adding a 20 MPa tensile stress). Subtracting the bending stress due to air flow pressure (7 MPa) from this total magnitude of bending stresses, an additional bending stress of 63 MPa is estimated to have influenced the failure of the fan blades. This significant magnitude of additional bending stress, probably caused by excessive vibrations, can explain the early initiation and rapid growth of fatigue cracks to final fracture in the fan blades, which occurred after only a short period of operation following the last overhaul.

The final fatigue crack of the second fractured blade (blade No. 8) is similar to blade No.1 and can be assumed as a quarter-elliptical corner crack too with $a = 11\times10^{-6}$ m and $c = 71\times10^{-6}$ m dimensions. According that, the values for F, H and Q parameters were

calculated as 3.74, 0.24 and 1.07 respectively for this crack. With similar calculations as before the bending stress at the time of final fracture for blade No. 8 can be estimated as 115 MPa and the total stress acting on this airfoil is about 135 MPa.

Finally, for the third fractured blade (blade No. 11), the final fatigue crack shape is different and can be assumed as a semi-elliptical surface crack with $a = 11 \times 10^{-6}$ m and $c = 55 \times 10^{-6}$ m dimensions. After calculation of the crack geometry parameters (F=1.84, H=0.66, Q=1.10) and using the Eq. (3), the bending stress at the time of final fracture for this blade was estimated as 118 MPa. By adding a 20 MPa tensile stress, the total stress is thus about 138 MPa. The details of above calculations can be found elsewhere (Sameezadeh, 2005; Ataei, 2006). Table 4 shows the summary of stress analysis results for the fan blades. According to the estimated failure stresses for the fractured blades it should be noted that the significant magnitude of additional stresses acting on the blades and leading to the premature and catastrophic failure of the fan, possibly have been due to aerodynamical disturbances that have resulted in a state of resonant condition of vibration. Additionally, changes in blade installation conditions, such as the level of torque tightening applied to the fixing bolts, which can influence the blade natural frequency, may be regarded as a contributing factor to fan blade failure shortly after overhaul.

	Centrifugal tensile stress (MPa)	Total bending stress (MPa)	Additional bending stress (MPa)	Maximum stress (MPa)
Normal condition	20	7	0	27
Blade No. 1	20	70	63	90
Blade No. 8	20	115	108	135
Blade No. 11	20	118	111	138

Table 4. Summary of stress analysis results of the fan blades

3.5. Simulation of fatigue crack growth

Fatigue crack growth rates in a model of the airfoils, under the action of estimated loads, were computed using FRANC3D/BES crack propagation software. The FRANC3D (FRacture ANalysis Code for 3D problems)/BES (boundary element solver) software developed at cornell university, is capable of evaluating stress intensity factors (SIF) along 3D crack fronts. This software utilizes boundary elements and linear elastic fracture mechanics. The displacements and stress intensity factors are calculated on the crack leading edge to obtain crack propagation trajectories and growth rates. It was assumed throughout the calculations that linear elastic fracture mechanics conditions hold (Carter et al., 2000; Cornell Fracture Group [CFG], 2002).

A simplified 3D model of airfoils was created using a geometry pre-processor program called OSM (Object Solid Modeler). A boundary element model of the geometry, consisting of triangular and square elements was then meshed within the FRANC3D program, and the stresses were applied by the model boundary conditions.

To start the crack growth simulation in FRANC3D an initial crack was introduced into the model. The initial crack was assumed to be a semi-elliptical surface crack with $\frac{a}{c} = 0.1$, based on previous fractographic findings. Initial crack length was computed from the threshold stress intensity factor range based on the equation (Hertzberg, 1989):

$$\Delta K_{\text{th}} = Y \Delta\sigma \sqrt{\pi a_0} \tag{7}$$

Taking ΔK_{th} from the literature and $\Delta\sigma$ values for the first and the second fractured blades based on the computed failure stresses and the positive portion of the stress cycle, and using the calculated values of Y from Newman–Raju equations (Newman & Raju, 1984), the initial crack lengths below which crack growth is arrested, a_0, were computed to be approximately 48×10^{-5} m and 22×10^{-5} m for the first and the second fractured blades respectively.

Based on the stresses applied by the model boundary conditions, the initial crack was grown in a series of crack propagation steps. Fig. 15a is a simplified 3D model of the airfoil that was meshed 2D (Boundary elements) in FRANC3D for simulating fatigue crack growth in fractured blades. Fig. 15b shows simulated fatigue crack in blade No. 8 after three steps of propagation.

Stress intensity factors at each step were calculated within FRANC3D and the fatigue crack growth curves were calculated using the Paris power law relationship given by (Broek, 1995):

$$\frac{\mathrm{d}a}{\mathrm{d}N} = C \Delta K^n \tag{8}$$

The empirical constants C and n were computed by fitting the near threshold crack growth data for AA 2124 aluminum alloy (Department of Defense, 1998) as $C = 9.5 \times 10^{-13}$ m.(MPa$\sqrt{\text{m}}$)$^{-\text{n}}$ and $n = 4.9$ for da/dN expressed in m.cycle^{-1} at a load ratio of $R = -0.1$ assumed in this case. The results of crack growth simulations in the first and the second fractured blades, where initial cracks are grown in small steps to their final dimensions are plotted in Fig. 16. These curves show the crack size as a function of the number of applied stress cycles. It can be seen that the number of cycles required to propagate initial cracks to their final dimensions for the first and the second fractured blades are just about 1.3×10^6 and 8×10^5 cycles respectively.

Stress calculations showed that the total stress acting on the third fractured blade (blade No. 11) is higher than for the two other fractured blades. Therefore, it can be assumed that the fatigue crack growth life of this blade is the shortest one and has the least portion on the total fatigue crack growth life of the failed fan. Thus, the simulation of blade No. 11 fatigue crack growth life was not performed and was ignored.

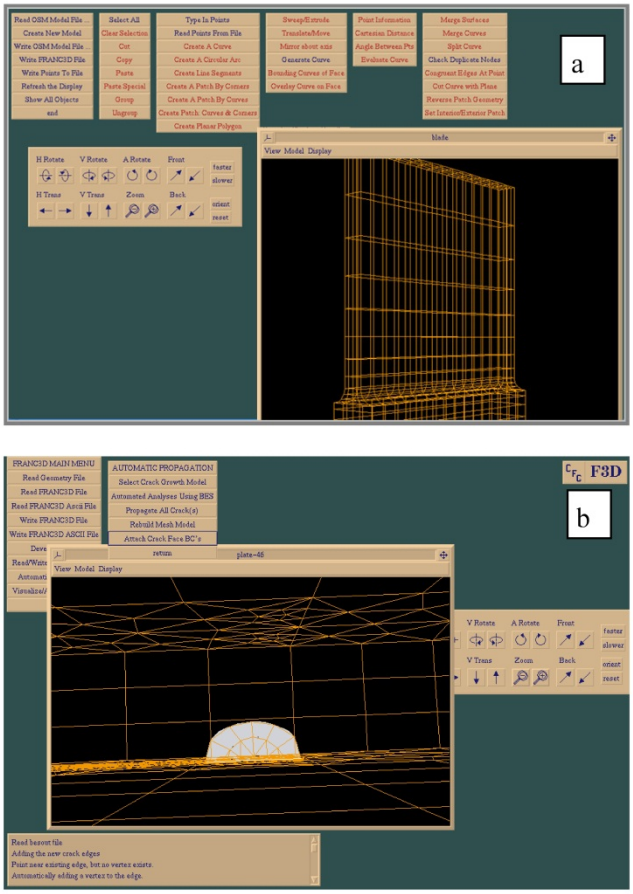

Figure 15. (a) A 3D model of the airfoil with 2D mesh for simulating fatigue crack growth in FRANC3D software and (b) simulated fatigue crack in blade No. 8 after three steps of propagation

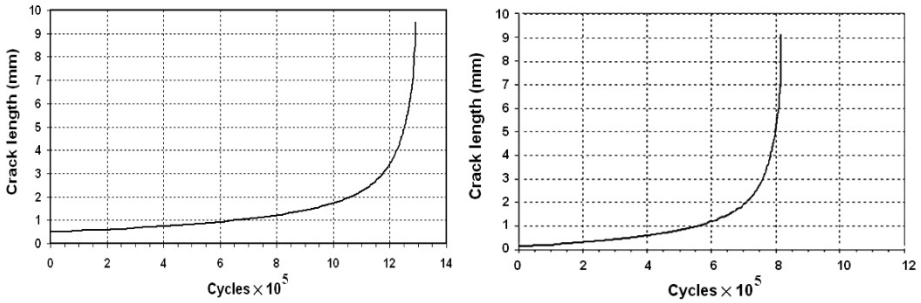

Figure 16. Crack length as a function of number of cycles in: (a) the first fractured blade (blade No. 1) and (b) the second fractured blade (blade No. 8)

As mentioned before, it is assumed that the excessive vibrations of the fan blades resulted from a resonant condition. Therefore, modal analysis was performed and natural frequencies and corresponding mode shapes were calculated. The results show that the first bending vibrational mode is a possible cause of the blades' failure. This first natural frequency calculated as 649 Hz (Ataei, 2006) So, the fatigue crack growth time for the first fractured blade with respect to the first natural frequency value (649 Hz) can be calculated as below:

$$t_{g1} = \frac{1.3 \times 10^6}{649 \times 3600} = 0.56 \quad hour \quad ` \tag{9}$$

and similarly for the second fractured blade:

$$t_{g2} = \frac{8 \times 10^5}{649 \times 3600} = 0.34 \quad hour \tag{10}$$

Thus the total fatigue crack growth time is about one hour. This lifetime is within the 11 hours of actual operating period following the last overhaul, which ended with the failure of fan blades.

4. Conclusion

1. Based on fractographic observations, high cycle fatigue was identified as the primary cause of failure of fan blades.
2. Fatigue cracks initiated at large second phase particles.
3. Premature fatigue failure of the fan blades was caused by significant levels of additional bending stresses, probably due to excessive vibrations resulting from resonance.
4. The failure stress for the first fractured blade was estimated to be about 90 MPa, which is significantly higher than the normal operating stress (more than three times higher).

5. Based on crack growth simulations in the first and the second fractured blades, the total fatigue crack growth time was calculated as only about one hour, which is within the 11 hours of actual operating period following the last overhaul, ending with the failure of fan blades.

Nomenclature

A	cross-sectional area, m^2
a	crack depth, m
a_0	initial crack depth, m
c	length for corner cracks and half-length for surface cracks
a/c	crack aspect ratio
F	boundary correction factor on stress intensity factor for remote tension
H	bending multiplier on stress intensity factor for remote bending
K_{IC}	critical stress intensity factor, $\text{MPa}\sqrt{\text{m}}$
K_t	stress intensity factor due to tension, $\text{MPa}\sqrt{\text{m}}$
K_b	stress intensity factor due to bending, $\text{MPa}\sqrt{\text{m}}$
m	mass of blade, kg
N	rotational speed, revolutions per second
Q	crack shape factor
r	distance from center of rotation, m
t_g	fatigue crack growth time, hours
σ_t	tensile stress, MPa
σ_b	bending stress, MPa
$\Delta\sigma$	stress range, MPa
ΔK_{th}	threshold stress intensity factor range, $\text{MPa}\sqrt{\text{m}}$
ΔK	stress intensity factor range, $\text{MPa}\sqrt{\text{m}}$
$\frac{da}{dN}$	crack growth rate , m.cycle^{-1}
C	empirical material constant
n	empirical material constant

Author details

Mahmood Sameezadeh and Hassan Farhangi
University of Tehran, College of Engineering, Iran

Acknowledgement

The authors are grateful to Eng. H. Vahedi and Dr. E. Poursaeidi of the Iran Power Plant Repairs Company (IPPRC) for their support and stimulating discussions. The authors also acknowledge the helpful assistances of Eng. M. Vatanara and Eng. P. Ataei during the study.

5. References

American Society for Metals [ASM]. (1990), *ASM Handbook*, Vol. 2, 10th ed., ASM International, OH, ISBN o-87170-378-5

Anderson, T. (1995). *Fracture Mechanics Fundamental and Applications*, 2nd ed., CRC Press, ISBN 978-0849342608, Texas

Ataei, P. (2006). *Fatigue Fracture and Life Evaluation of Generator Rotor Fan Blades of a Thermal Power Plant*, MSc thesis, Islamic Azad University, South Tehran Branch, Iran

Bleier, F.P. (1997). *Fan Handbook, Selection, Application and Design*, McGraw-Hill, ISBN 978-0070059337, New York

Broek, D. (1995). *The Practical Use of Fracture Mechanics*, Kluwer Academic Publisher, ISBN 978-0792302230 ,OH

Carter, B.J.; Wawrzynek, P.A. & Ingrafera, A.R. (2000). Automated 3-D Crack Growth Simulation, International Journal for Numerical Methods in Engineering, Vol. 47, pp. 229-253, ISSN 0029-5981

Cornell Fracture Group [CFG]. (2002). *FRANC3D, Menu & Dialog Reference V2.2*, Cornell University, USA

Cornell Fracture Group [CFG]. (2002). *OSM, Menu and Dialog Reference V2.2*, Cornell University, USA

Department of Defense. (1998). *Metallic Materials and Elements for Aerospace Vehicle Structures*, MIL-HDBK-5H, New York

Hertzberg, R.W. (1989). *Deformation and Fracture Mechanics of Engineering Materials*, 3rd ed., Wiley, ISBN 978-0471012146, New York

Iran Power Plant Repair Company [IPPRC], (2003). *Failure Analysis Report of Iran-Neyshabour Unit 2B*, Iran

Iran Power Plant Repair Company [IPPRC], (2004). *Failure Analysis Report of Iran- Montazer-Ghaem Unit 4*, Iran

Koul, A.K. & Dainty, R.V. (1992). Fatigue fracture of aircraft engine compressor disks, In: *Handbook of Case Histories in Failure Analysis,* Vol. 1, K.A. Esaklul, pp. 241-245, ASM international, ISBN 978-0-87170-453-5, USA

Kung, C.Y. & Fine, M.E. (1979). Fatigue crack initiation and microcrack growth in 2024-T4 and 2124-T4 aluminum alloys, *Metallurgical and Materials Transactions A*, Vol. 10, pp. 603-610, ISSN 1073-5623

Merati, A. (2005). A study of nucleation and fatigue behavior of an aerospace aluminum alloy 2024-T3, *International Journal of Fatigue*, Vol. 27, pp. 33-44, ISSN 0142-1123

Moore, W.G. (2002). Several Case Histories of Generator Rotor Fan Failures and Methods of Repair, *Proceedings of international joint power generation conference*, ASME committee (Ed.), Phoenix, 2002

Moussavi, S.E.; Yadavar, S.M. & Jahangiri, A. (2009). Failure analysis of gas turbine generator cooling fan blades. *Engineering Failure Analysis*, Vol. 16, pp. 1686-1695, ISSN 1350-6307

Newman, J.C. & Raju, I.S. (1984). *Stress-intensity Factor Equations for Cracks in Three-dimensional Finite Bodies Subjected to Tension and Bending Loads*, NASA technical memorandum 85793, NASA, Virginia

Sameezadeh, M. (2005). *Analysis of Fatigue Failure of Generator Rotor Fan Blades*, MSc thesis, School of Metallurgy and Materials Engineering, University of Tehran, Iran